JASA ARTICLE

Tunable network sound absorber based on additive manufacturing[a)]

Tianyu Zhao, Yi Chen, Kai Zhang,[b)] and Gengkai Hu[c)]
School of Aerospace Engineering, Beijing Institute of Technology, Beijing 100081, China

ABSTRACT:
Broadband sound absorption at low frequencies is always a challenge owing to the strong penetrability of acoustic waves. Combining detuned components, such as coupling curled Fabry–Pérot channels, has been proposed for broadband sound absorption. However, the components of the structure are generally arranged in parallel, so that it is difficult to assemble channels with gradient lengths into a compact and thin absorber. Tube networks, which can be seen as broadband and low-frequency sound absorbers, can circumvent this problem. However, the network absorber can only work at fixed frequencies once fabricated. Here, we propose a tunable low-frequency sound absorber consisting of honeycomb plates and detached chips and fabricate it by additive manufacturing. By replacing chips of the sound absorber, we experimentally validate different sound absorption spectrums. A low reduced frequency model and genetic algorithm are developed to design the chips according to targeted absorption spectrums. Moreover, we theoretically study the impact of radius of tube on sound absorption and extend the two-dimensional network to a three-dimensional structure. The remarkable efficiency and versatility of the tunable network sound absorber may pave the way for programmed absorbing material design.
https://doi.org/10.1121/10.0005507

(Received 21 March 2021; revised 27 May 2021; accepted 10 June 2021; published online 7 July 2021)

[Editor: Christina Jeanne Naify] Pages: 94–101

I. INTRODUCTION

Noise reduction is necessary for human health in many working and living scenarios. Conventional sound absorbers, such as porous and fibrous materials (Allard and Atalla, 2009; Biot, 1956; Huang *et al.*, 2014), generally require a structural thickness comparable to wavelength, which results in bulky structures for low-frequency noises. Micro-perforated panels with backed cavities can absorb low-frequency sound efficiently but still suffer from a large thickness of the back cavity (Maa, 1975, 1998; Toyoda *et al.*, 2011; Wu *et al.*, 2019). During recent decades, acoustic metamaterials (Fang *et al.*, 2006; Liu *et al.*, 2000; Huang and Sun, 2010) and metasurfaces (Li *et al.*, 2015; Xie *et al.*, 2014) with a sub-wavelength thickness have shown tremendous functionalities of acoustic wave control, such as negative refraction (Kaina *et al.*, 2015; Liang and Li, 2012; Xie *et al.*, 2013), deep sub-wavelength focusing/imaging (Christensen and Javier García de Abajo, 2012; Li *et al.*, 2009; Zhu *et al.*, 2011), and cloaking (Chen *et al.*, 2017; Popa *et al.*, 2011). Particularly, sound-absorptive metamaterials consisting of resonant units, such as membrane-type resonators (Ma *et al.*, 2014; Mei *et al.*, 2012), Helmholtz resonators (Cai *et al.*, 2014; Chen *et al.*, 2017; Ryoo and Jeon, 2018), and Fabry–Pérot (FP) channels (Jiang *et al.*, 2014; Yang *et al.*, 2017), can realize even high sound absorption at targeted low frequencies. However, due to the dispersive nature of the resonances, narrowband performance largely hinders their applications.

To obtain broadband absorption, one feasible way is to combine several detuned components together. Yang *et al.* (2017) used curled FP channels to form an optimal sound absorption structure. The components of the structure are generally arranged in parallel, so it is difficult to assemble the channels with gradient lengths into a compact and thin absorber (Huang *et al.*, 2018). Designing tube networks inside a cubic can circumvent this problem (Cambonie and Gourdon, 2018, van der Eerden, 2000). However, the tube network absorber can only work well at fixed frequencies once fabricated. Tunable sound-absorbing metamaterials have been realized by embedding functional structures into metamaterials, such as apertures (Huang *et al.*, 2019), Mie resonators (Shao *et al.*, 2021), and panels (Wang *et al.*, 2018). Additive manufacturing techniques are suitable for the implementation of tunable sound-absorbing metamaterials (Cavalieri *et al.*, 2021; Ngo *et al.*, 2018; Zhang *et al.*, 2016). Here, we propose a tunable sound absorber consisting of optimized tube networks based on additive manufacturing. The key to achieving tunability is to decompose a generalized tube network into two types of elements: honeycomb plates and chips, as shown in Fig. 1. The honeycomb panels consist of multiple identical tubes arranged in parallel, of which the length is equal to the thickness of the honeycomb panels. The chips can control the opening and closing of each tube in the honeycomb plate as well as the

[a)]This paper is part of a special issue on Additive Manufacturing and Acoustics.
[b)]Electronic mail: zhangkai@bit.edu.cn
[c)]Electronic mail: hugeng@bit.edu.cn

 0001-4966/2021/150(1)/94/8/$30.00

connectivity of adjacent tubes in the honeycomb plate. Given fixed honeycomb plates, we tune the sound absorption performance of the network absorber by simply changing its chips. The low reduced frequency model and genetic algorithm (GA) are used to design the chips, according to targeted absorption spectrums. We design different groups of chips, which are fabricated by three-dimensional (3D) printing technology, and experimentally validate the targeted low-frequency sound absorption spectrums. Based on the optimized network absorber, we realize broadband and low-frequency sound absorption. The remarkable efficiency and versatility of tunable network sound absorbers may pave the way for programmed absorbing material design.

The paper is organized as follows: In Sec. II, a theoretical model for sound absorption of a tube network and numerical algorithm for optimizing the tube distribution are introduced. The theoretical model is validated through experiments. Section III is concerned with designing network absorbers according to various optimizing targets, including broadband absorption and specific absorption at specified frequency ranges. The low-frequency sound absorption performance of the tunable absorber is experimentally validated in Sec. III. The impact of the radius of tubes on absorption and the 3D structure of the network are discussed at the end of Sec. III. The main findings and conclusions are finally summarized in Sec. IV.

II. METHODS

A. Theory

Sound absorption in a tube originated from thermal and viscous effects of air can be characterized by a low reduced frequency model (Tijdeman, 1975; Zwikker and Kosten, 1949), which is briefly recalled in the following. Consider a tube with length l [Fig. 2(a)], of which two ends are denoted as i and j. According to the low reduced frequency model, acoustic pressure $p(x)$ and velocity $v(x)$ at location x in the tube [see Fig. 2(a)] with circular frequency ω can be analytically described,

$$p(x) = p_A \exp(\Gamma k_0 x) + p_B \exp(-\Gamma k_0 x), \tag{1}$$

$$v(x) = \frac{G}{\rho_0 c_0}(p_A \exp(\Gamma k_0 x) - p_B \exp(-\Gamma k_0 x)), \tag{2}$$

in which p_A and p_B can be regarded as the incident and reflection coefficient, ρ_0 and c_0 denote the density and sound velocity of air, respectively, and $k_0 = \omega/c_0$ is the wave number. Parameters G and Γ are defined as

$$G = -i\gamma/(\Gamma n), \quad \Gamma = \sqrt{\frac{J_0(i\sqrt{i}s)\gamma}{J_2(i\sqrt{i}s)n}},$$
$$n = \left(1 + \frac{(\gamma-1)J_2(i\sqrt{i}s\sigma)}{J_0(i\sqrt{i}s\sigma)\gamma}\right)^{-1}, \tag{3}$$

where J_0 and J_2 are Bessel functions of the first kind of order 0 and 2, respectively. Parameter $s = R(\rho_0\omega/\mu)^{1/2}$ is the shear wave number, with μ denoting the dynamic viscosity (18.2×10^{-6} Ns/m^2); the square root of the Prandtl number σ is 0.84, and the specific heat γ is 1.4. R denotes the radius of the tubes.

Mass flow disturbances at both ends of the tubes are $Q_i = \rho_0 A v_i$ and $Q_j = -\rho_0 A v_j$, where v_i and v_j are the acoustic velocity at both ends, and A is the cross section area of the tube. With the pressure and velocity distributions in Eqs. (1) and (2), the two mass flow disturbances are related to pressures at both the ends,

$$\begin{pmatrix} Q_i \\ Q_j \end{pmatrix} = \frac{AG}{c_0 \sinh(\Gamma k_0 l)} \begin{pmatrix} -\cosh(\Gamma k_0 l) & 1 \\ 1 & -\cosh(\Gamma k_0 l) \end{pmatrix} \begin{pmatrix} p_i \\ p_j \end{pmatrix}, \tag{4}$$

in which p_i and p_j are the pressure disturbances at the two ends. The low reduced frequency model is generally expressed in terms of such a transmission relation. If the two end pressures are known, the pressure and velocity distributions in the tube can be obtained.

To verify the accuracy of the low reduced frequency model, we calculate the sound absorption performance of a cylinder tube using the narrow region acoustics of the pressure acoustics module in COMSOL Multiphysics® 5.5. We used three-node plane solid elements. As shown in Fig. 2(e), the tube ends up with a hard wall, of which the length is 200 mm and the diameter is 5 mm. The surface porosity of the tube is 1/8. The numerical result agrees well with the theoretical result.

Figure 2(b) shows a tube network, in which every horizontal and vertical line represents a tube. The network has $(m-1) \times n$ nodes and $2mn - m - 3n + 2$ tubes. To calculate the sound absorption of the tube network, a plane wave is incident from the left side. Under low-frequency

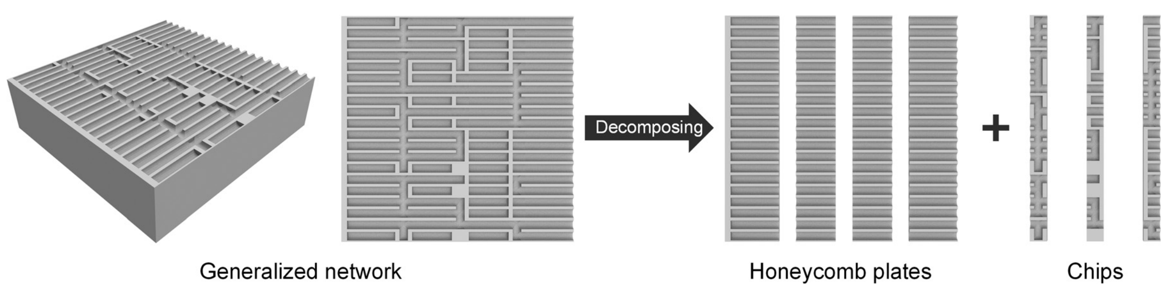

FIG. 1. Decomposing the network absorber into honeycomb plates and chips.

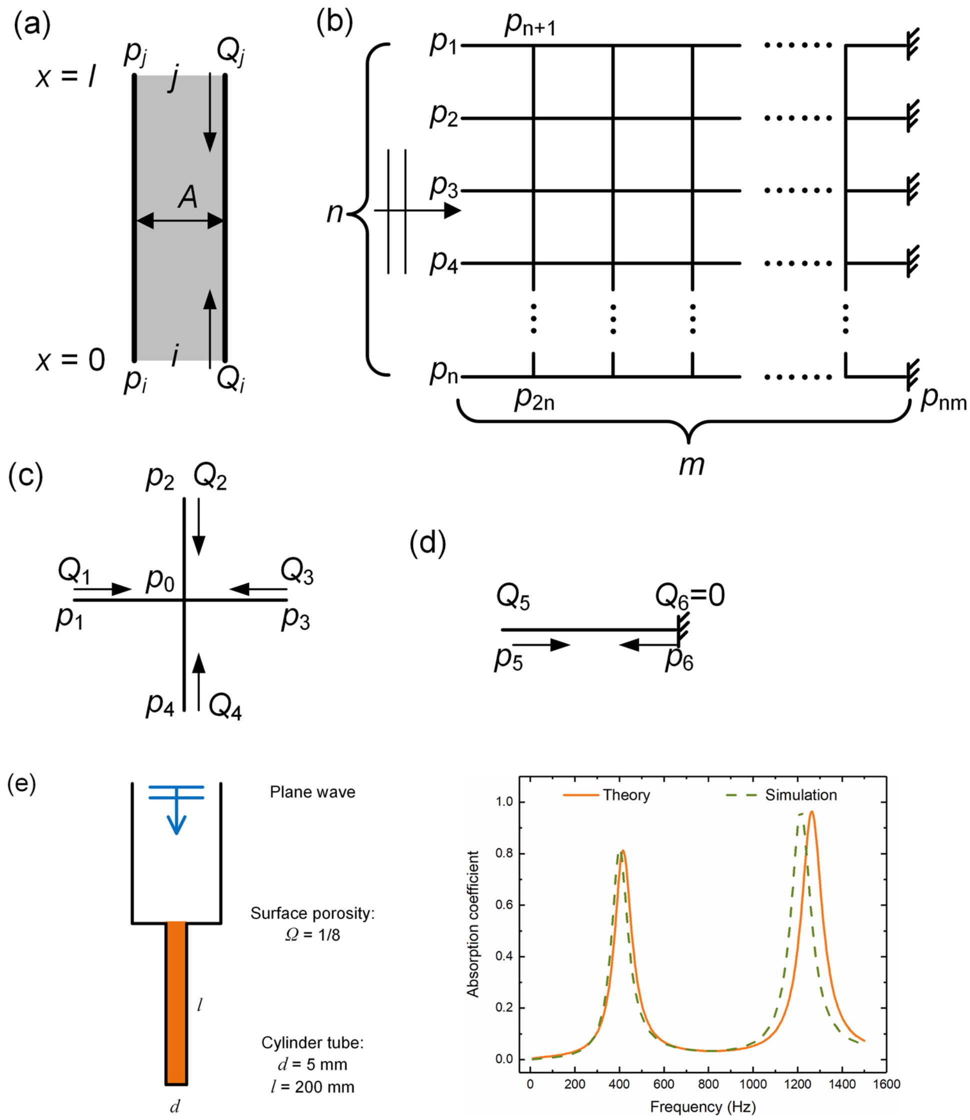

FIG. 2. (Color online) (a) Low reduced frequency model for wave propagation in a tube; (b) tube network; (c) scheme of mass conservation law at nodes; (d) mass conservation law at sound hard wall; (e) comparing sound absorption performance results of a cylinder tube obtained by numerical method/theoretical method, respectively.

conditions, pressures at the entrance of the tubes are the same and supposed to be unit $p_k = 1\,\text{Pa}$ ($k = 1, 2\ldots n$). The pressures at other tube ends are called node pressure. The tube network has in total $(m-1)\times n$ unknown node pressures p_k ($k = n+1, n+2\ldots nm$). For each node connecting more than one tube as illustrated in Fig. 2(c), a conservation law holds for the mass flow disturbance,

$$\sum_{k=1}^{4} Q_k + \frac{i\gamma k_0}{c_0 n} p_0 V = 0. \tag{5}$$

Q_k can be obtained from two node pressures of each tube, and $V = 16R^3/3$ is the intersecting volume of multiple circular tubes. We can construct a linear equation in terms of node pressure p_k for each node, and $(m-2)\times n$ equations can be obtained. For tubes terminated with the sound hard wall shown in Fig. 2(d), the mass flow disturbance at the right side of the tube is zero,

$$Q_6 = p_5 - \cos(\Gamma k_0 l) p_6 = 0. \tag{6}$$

In total, n equations for zero mass flow can be obtained for the above model. Now the number of equations and the number of unknown node pressures are the same, $(m-1)\times n$. These equations can be assembled into a matrix equation,

$$\mathbf{M}(p_{n+1}, p_{n+2}\ldots p_{2n}, \ldots p_{nm})^{\mathrm{T}} = \mathbf{f}(p_1, p_2, \ldots p_n). \tag{7}$$

$\mathbf{M}$ is a square matrix of dimension $(m-1)n \times (m-1)n$, and $\mathbf{f}$ is a column vector depending on the entrance pressure $p_k = 1$ ($k = 1, 2\ldots n$). The unknown node pressures can then be solved from Eq. (7), and the normalized surface impedance at the entrance of the tube network is obtained,

$$\frac{1}{Z^{\mathrm{eff}}} = \sum_{k=1}^{n} \frac{\Omega}{Z_k}, \quad Z_k = \frac{-G}{\rho_0 c_0}\frac{p_k}{\nu_k} = \frac{-GA}{c_0}\frac{p_k}{Q_k}. \tag{8}$$

Here, Ω is the surface porosity of the tube network. The mass flow Q_k can be obtained according to Eq. (4). The sound absorption coefficient is derived from the normalized surface impedance,

$$\alpha = \frac{4\mathrm{Re}(Z^{eff})}{\left(1+\mathrm{Re}(Z^{eff})\right)^2 + \left(\mathrm{Im}(Z^{eff})\right)^2}. \tag{9}$$

It is noted that the above method is also applicable if any tube in the network is removed. In addition, we add $0.8R$ to the length of each tube to represent the thickness of chips.

GA in MATLAB is adopted to optimize the distribution of the tubes according to the targeted absorption spectrum. GA is an optimization algorithm that searches for the global optimal solution and does not need the derivative of the objective function (Goldberg and Holland, 1988). First, randomly generate the initial population of individuals, which are parents. Next, evaluate the fitness of each individual in that population. Then select the best-fit individuals for reproduction and generate new individuals through crossover and mutation operations in parents. If a fixed number of the generations are finished, then stop and return the optimized result. Otherwise, go to the next generation. During the optimization design of the network absorber, the objective function is the average sound absorption of the target frequency range. We use the default parameter settings of GA in MATLAB R2017b. For the optimization design of the network absorber in Fig. 3, the optimization variables form a 1×117 binary sequence. The population size is 200. The crossover probability is 0.8, and the mutation probability is 0.005. We emphasize here that the combination of the low reduced frequency model and GA is quite flexible to design tube networks for the programmed absorption spectrum. As demonstrated in Sec. III, it is hardly achieved with current absorption design strategy based on porous materials or perforated plate technique.

B. Experiments

We design and fabricate an optimized network absorber and experimentally measure its absorption performance. The optimization target is complete absorption from 500 to 800 Hz. As shown in Fig. 3(a), the total thickness of absorber is assumed to be 82 mm ($\lambda/5$), of which 2 mm is the thickness of hard boundary. According to the precisions of experimental equipment and printing equipment, the area of incident surface is set to be $79.3 \times 79.3\ \mathrm{mm}^2$, and the radius of tubes is set as 1.5 mm. There are in total 20 tubes at the incident surface in a single layer of network; therefore, the distance between adjacent rows is 0.965 mm. The network absorber consists of 20 identical layers of tube network, of which the distance between adjacent layers is 0.965 mm. The network absorbers are fabricated by 3D printing (SR600SS, Uniontech, China) using DSM's Somos® Imaging 8000 (DSM Functional Materials, Elgin, IL) as matrix (Young's modulus: 2.2 GPa, density: $1200\ \mathrm{kg/m}^3$). The measurements of the absorption coefficients are performed using the two-microphone transfer-function method [Brüel & Kjaer (Naerum, Denmark) type-4206T] according to ISO 10534–2 (1998) to obtain the sound absorption spectrums. We fabricate an impedance tube with a rectangle cross section ($79.7 \times 79.7\ \mathrm{mm}^2$) using aluminum alloy. During the experiments, the absorber is tightly stuck in the impedance tube, which is end up with a hard wall. The distance between two microphones is 5 cm. The cut-off frequency of the impedance tube is 2151 Hz.

III. RESULTS

The structure of the absorber consists of 20 identical layers of tube networks, and the results of absorption performance of the absorber are shown in Fig. 3. The red solid line represents the results predicted by the low reduced frequency model, and the blue dashed line represents the experimental results. The two lines agree well at resonant frequencies. The theoretical average absorption from 500 to 800 Hz is 86.8%, and measured average absorption from 500 to 800 Hz is 84.1%, realizing broadband and low-frequency sound absorption with a sub-wavelength thickness.

Afterward, we experimentally demonstrate the tunable network sound absorber. The absorber is decomposed into

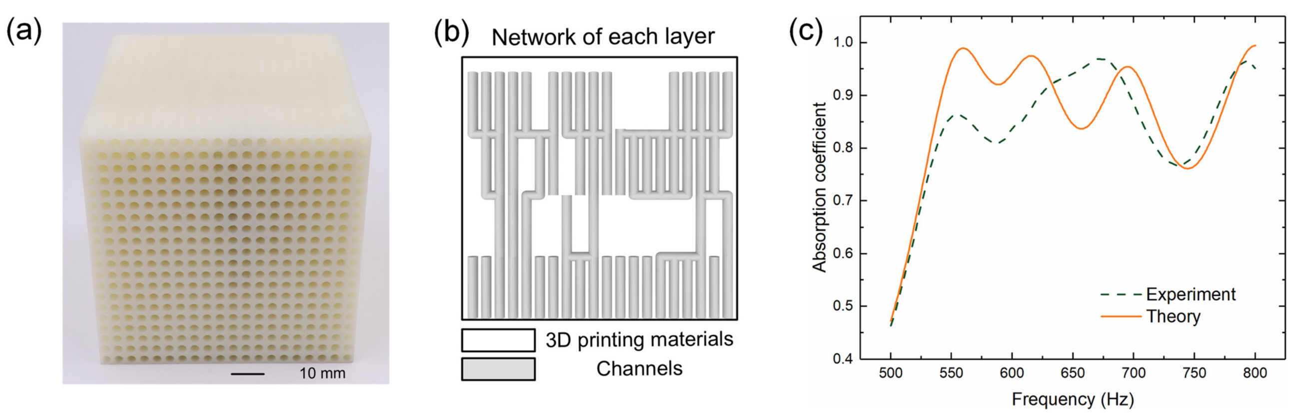

FIG. 3. (Color online) (a) The structure of the absorber consists of 20 identical layers of tube networks; (b) the network in each layer. (c) The red solid line represents the sound absorption coefficient of network predicted by theory, and the blue dashed line represents the experimental result.

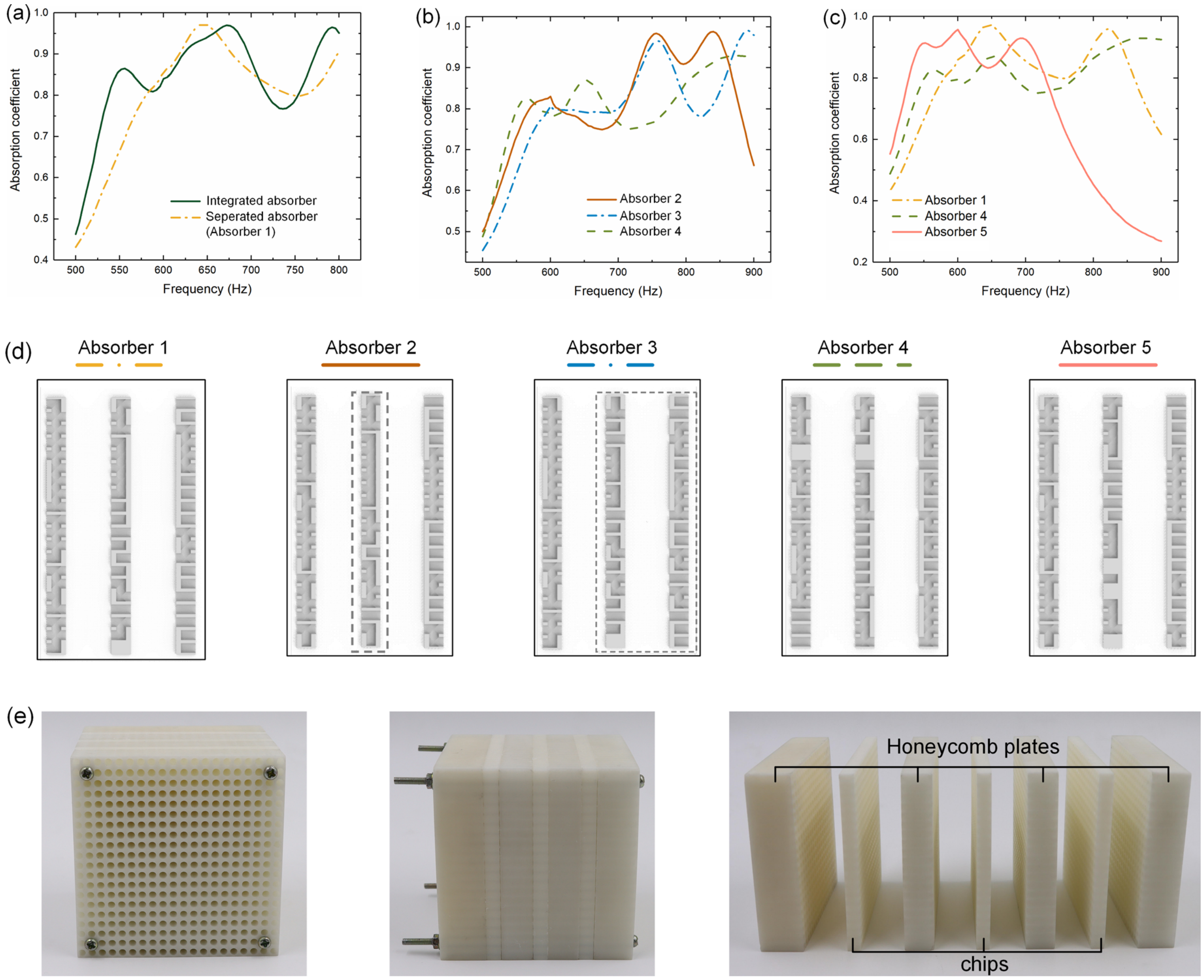

FIG. 4. (Color online) (a) Comparison between integrated absorber and separated absorber. (b) Changing chips to increase the distance between the two peaks. (c) Changing chips to increase the absorption bandwidth. (d) Corresponding absorbers 1–5. (e) The separated absorber consists of honeycomb plates and chips.

seven parts, including three chips and four honeycomb plates, as shown in Fig. 4. To obtain different targeted sound absorption spectrums, we can change chips in the absorber. For example, we assemble a tunable network sound absorber [absorber 1 in Fig. 4(d)], whose network is the same as the "integrated" network shown in Fig. 3. The sound absorption performance of the tunable network is experimentally measured and represented by the yellow line in Fig. 4(a). There

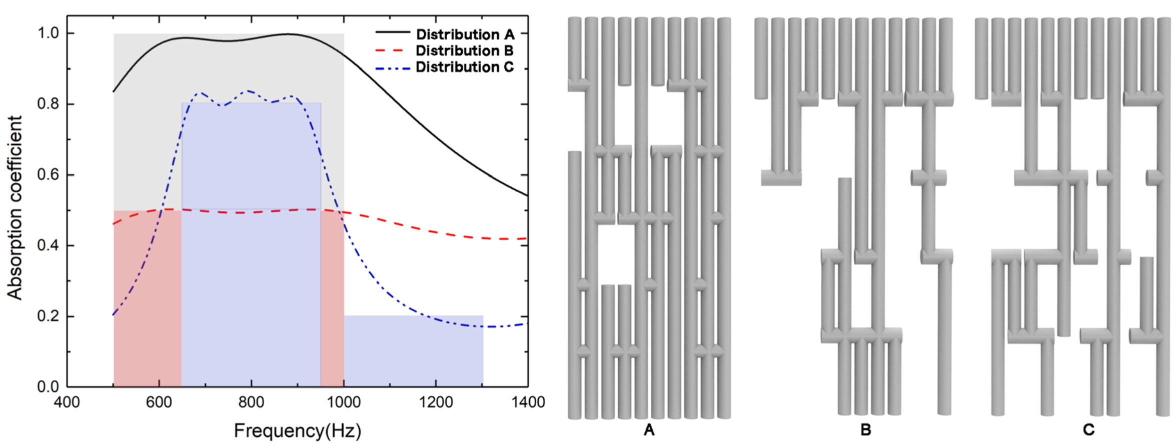

FIG. 5. (Color online) Three low-frequency absorption targets are described by the gray zone (100% absorption from 500 to 1000 Hz), red zone (50% absorption from 500 to 1000 Hz), and blue zones (80% absorption from 650 to 950 Hz and 20% absorption from 1000 to 1300 Hz). Three optimized absorption results are described by the black solid line (network **A**), red dashed line (network **B**), and blue dashed-dotted line (network **C**).

TABLE I. Geometric parameters of six optimized networks.

	A	B	C	D	E	F
R (mm)	0.3	0.2	0.7	0.2	0.1	0.2
L (mm)	0.1	0.2	0.7	0.05	0.1	0.1
H (mm)	0.1	0.3	0.75	0.05	0.1	0.1
m	6	5	5	5	5	5
n	9	11	11	11	11	11

exists some discrepancy of the sound absorption performance, which indicates that there are some small gaps between the honeycomb plates and chips. Overall, the tunable network works well at the designed frequency band, and its performance is consistent with its "integrated" version.

By changing the chips in the absorber, we assemble three different absorbers, and the corresponding sound absorption performances are measured, as shown in Fig. 4(b). For absorber 2 [Fig. 4(d)], the sound absorption peaks are located at 756 and 836 Hz. Compared with absorber 2, the two peaks of absorber 3 [Fig. 4(d)] with one different chip move away from each other (760 and 890 Hz). We further change one chip to form absorber 4 [Fig. 4(d)], for which the distance between two peaks becomes larger (650 and 870 Hz). We conclude that by changing chips, we can adjust the distance between two absorption peaks.

The absorber 4 shown in Fig. 4(d) is used for absorption from 500 to 900 Hz, and absorber 5 shown in Fig. 4(d) is used for absorption from 500 to 700 Hz. We experimentally obtain the sound absorption performance of the two absorbers, as shown in Fig. 4(c). It can be seen that the absorption peaks of the three absorbers (absorbers 1, 4, and 5) fall in the designed frequency band, respectively. Thus, we conclude that the working frequency range of the absorber can be adjusted by changing the chips, which are guided by the low reduced frequency model and GA.

We theoretically investigate the broadband sound absorption based on the GA optimization of the tube network absorber. Diverse target sound absorption spectrums can be realized at low frequencies. For example, as shown in Fig. 5, we design three networks according to three absorption spectrum targets, respectively. The first target absorption spectrum is assumed to be 100% absorption from 500 to 1000 Hz. We obtain network **A** and its sound absorption performance, which is represented by the black solid line in Fig. 5. Then we reduce the target to half absorption over the same frequency range. It is realized by network **B**, whose absorption performance is represented by the red dashed line. Both the absorption performances of network **A** and **B** agree well with the target absorption spectrums, respectively. The third target absorption spectrum is assumed to be 80% absorption from 650 to 950 Hz and 20% absorption from 1000 to 1300 Hz, represented by the blue zones. Its optimized network **C** realizes 80% absorption from 650 to 950 Hz and 20% absorption from 1170 to 1300 Hz but is enabled to achieve more than 20% sound absorption from 1000 and 1170 Hz, as shown in Fig. 5. The lengths of the three networks **A–C** in the propagating direction are 80 mm, and other parameters of the three networks, including radius R, distance between rows L, distance between layers H, number of rows m, and number of columns n, are listed in Table I.

Apart from tailored low-frequency absorption, we can also design networks to realize a wider absorption spectrum. We design another three networks corresponding to three different absorption targets, respectively. As shown in Fig. 6, the gray zone represents the target of 100% absorption from 300 to 3000 Hz, and the black solid line represents the absorption performance of the corresponding network **D**. We can see the network **D** can reach 97%–99% absorption from 700 Hz, represented by the black solid line. Then we decrease the absorption target to 80% or 70% over the same frequency range, and the corresponding optimized network **E**/**F** can reach an 80%/70% absorption target from 700 Hz. The three networks **D–F** are of the same length, 120 mm in the incident direction, and other geometric parameters are listed in Table I.

We find that the tube radius significantly influences the absorption performance. To address the sound absorption

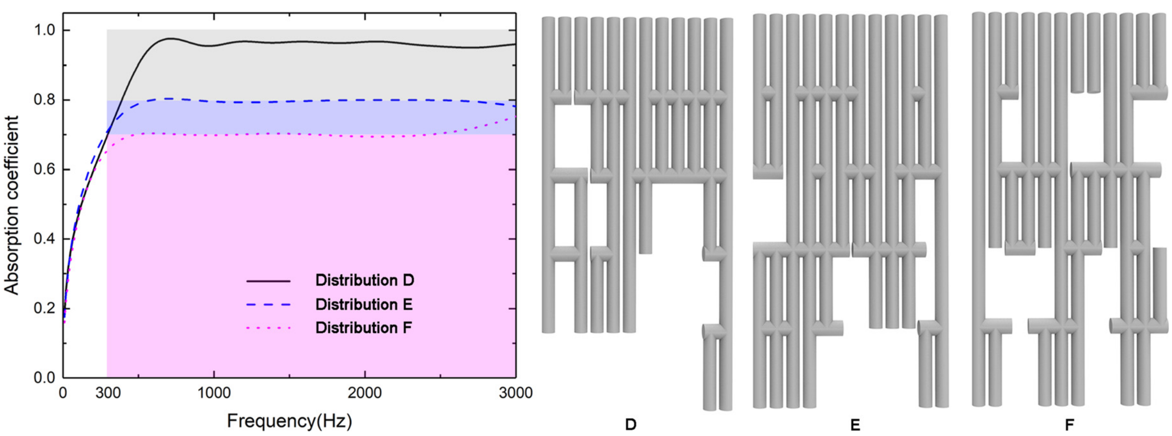

FIG. 6. (Color online) Three broadband absorption targets are described by the gray zone (100% absorption from 300 to 3000 Hz), blue zone (80% absorption from 300 to 3000 Hz), and red zones (70% absorption from 300 to 3000 Hz). Three optimized absorption results are described by the black solid line (corresponding to network **D**), blue dashed line (corresponding to network **E**), and red dotted line (corresponding to network **F**).

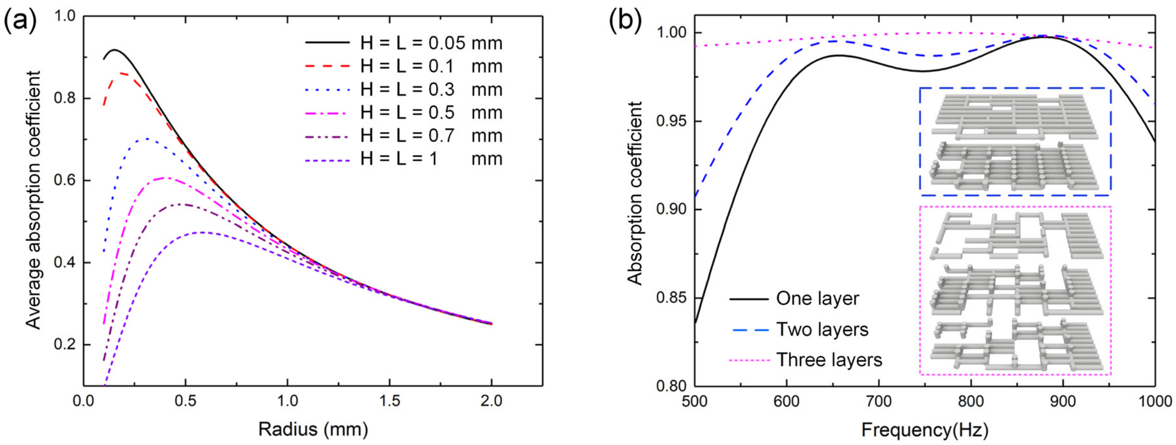

FIG. 7. (Color online) (a) The effect of radius on the average absorption. (b) The effect of 3D design on broadband absorption.

performance of a network with a different radius, we choose a "full" network, where all tubes are turned on, and consider the average absorption coefficient from 300 to 4000 Hz as an indicator of absorption performance. We change the radius of tubes and distances H and L. We set m to 4, n to 5, and thickness of network to 120 mm. We choose six cases for H and L and show how the absorption performances change with radius in Fig. 7(a). It can be seen that there exists one optimal radius corresponding to the best average absorption in every curve. The optimal radius decreases with the row distance H (layer distance L) decreasing. When H and L are less than 0.1 mm, the optimal radius value is around 0.15 mm, which is approximately equal to the boundary layer thickness of the tube at low frequency range (Cai *et al.*, 2018).

The above tube networks **A–F** are formed by identical layers, each of which is a two-dimensional (2D) network. For larger design space of optimization, we can add tubes at the nodes between two or more layers to optimize 3D networks. To compare with the one-layer network **A**, we design a two-layer network and a three-layer network to realize 100% absorption from 500 to 1000 Hz, which share the same geometric parameters. The networks and absorption results are all shown in Fig. 7(b). The red dotted line represents the results of the three-layer network, which is the best among the three networks. We conclude that 3D networks assembled with more different layers provide more paths for sound dissipation, having potentials for sound absorption.

IV. CONCLUSION

In this study, we propose and experimentally measure a tunable low-frequency sound absorber consisting of tube networks. The tube network can be optimized to provide broadband low-frequency absorption. We experimentally validate the optimized network, realizing 84.11% absorption from 500 to 800 Hz within an 82 mm thickness. By composing the network into honeycomb plates and chips, we can tune the absorption performance of the network absorber. Groups of chips are fabricated to carry out experiments on the tunable absorber. Furthermore, we found that there exists one optimal radius of tubes corresponding to best average absorption, and a 3D network can provide better absorption compared with a 2D network. The tunable network absorber has potential in new programmed absorbing material design.

ACKNOWLEDGMENTS

This work received funding support from the National Natural Science Foundation of China (Grant Nos. 11991030 and 11991031). We thank Q. Hu for help with the experiment. The authors declare that all relevant data and code supporting the findings of this study are available within the article or from the corresponding author on reasonable request. G.H. and K.Z. proposed the key idea of this paper. T.Z., K.Z., and Y.C. developed the method. T.Z. built the numerical program, carried out the numerical computation, and carried out the experiment. The authors declare no competing interests.

Allard, J., and Atalla, N. (**2009**). *Propagation of Sound in Porous Media: Modelling Sound Absorbing Materials*, 2nd ed. (Wiley, New York).

Biot, M. A. (**1956**). "Theory of propagation of elastic waves in a fluid-saturated porous solid. II. Higher frequency range," J. Acoust. Soc. Am. **28**, 179–191.

Cai, X., Guo, Q., Hu, G., and Yang, J. (**2014**). "Ultrathin low-frequency sound absorbing panels based on coplanar spiral tubes or coplanar Helmholtz resonators," Appl. Phys. Lett. **105**, 121901.

Cai, X., Yang, J., Hu, G., and Lu, T. (**2018**). "Sound absorption by acoustic microlattice with optimized pore configuration," J. Acoust. Soc. Am. **144**, 138–143.

Cambonie, T., and Gourdon, E. (**2018**). "Innovative origami-based solutions for enhanced quarter-wavelength resonators," J. Sound Vib. **434**, 379–403.

Cavalieri, T., Boulvert, J., Romero-García, V., Gabard, G., Escouflaire, M., Regnard, J., and Groby, J.-P. (**2021**). "Rapid additive manufacturing of optimized anisotropic metaporous surfaces for broadband absorption," J. Appl. Phys. **129**, 115102.

Chen, C., Du, Z., Hu, G., and Yang, J. (**2017**). "A low-frequency sound absorbing material with subwavelength thickness," Appl. Phys. Lett. **110**, 221903.

Chen, Y., Zheng, M., Liu, X., Bi, Y., Sun, Z., Xiang, P., Yang, J., and Hu, G. (**2017**). "Broadband solid cloak for underwater acoustics," Phys. Rev. B **95**, 180104.

Christensen, J., and Javier García de Abajo, F. (**2012**). "Anisotropic metamaterials for full control of acoustic waves," Phys. Rev. Lett. **108**, 124301.
Fang, N., Xi, D., Xu, J., Ambati, M., Srituravanich, W., Sun, C., and Zhang, X. (**2006**). "Ultrasonic metamaterials with negative modulus," Nat. Mater. **5**, 452–456.
Goldberg, D. E., and Holland, J. H. (**1988**). "Genetic algorithms and machine learning," Mach. Learn. **3**, 95–99.
Huang, G. L., and Sun, C. T. (**2010**). "Band gaps in a multiresonator acoustic metamaterial," J. Vib. Acoust. **132**, 031003.
Huang, S., Fang, X., Wang, X., Assouar, B., Cheng, Q., and Li, Y. (**2018**). "Acoustic perfect absorbers via spiral metasurfaces with embedded apertures," Appl. Phys. Lett. **113**, 233501.
Huang, S., Fang, X., Wang, X., Assouar, B., Cheng, Q., and Li, Y. (**2019**). "Acoustic perfect absorbers via Helmholtz resonators with embedded apertures," J. Acoust. Soc. Am. **145**, 254–262.
Huang, Y., Zhou, D., Xie, Y., Yang, J., and Kong, J. (**2014**). "Tunable sound absorption of silicone rubber materials via mesoporous silica," RSC Adv. **4**, 15171–15179.
ISO 10534-2 (**1998**). "Acoustics—Determination of sound absorption coefficient and impedance in impedance tubes—Part 2: Transfer-function method" (International Organization for Standardization, Geneva, Switzerland).
Jiang, X., Liang, B., Li, R., Zou, X., Yin, L., and Cheng, J. (**2014**). "Ultra-broadband absorption by acoustic metamaterials," Appl. Phys. Lett. **105**, 243505.
Kaina, N., Lemoult, F., Fink, M., and Lerosey, G. (**2015**). "Negative refractive index and acoustic superlens from multiple scattering in single negative metamaterials," Nature **525**, 77–81.
Li, J., Fok, L., Yin, X., Bartal, G., and Zhang, X. (**2009**). "Experimental demonstration of an acoustic magnifying hyperlens," Nat. Mater. **8**, 931–934.
Li, Y., Jiang, X., Liang, B., Cheng, J., and Zhang, L. (**2015**). "Metascreen-based acoustic passive phased array," Phys. Rev. Appl. **4**, 024003.
Liang, Z., and Li, J. (**2012**). "Extreme acoustic metamaterial by coiling up space," Phys. Rev. Lett. **108**, 114301.
Liu, Z. Y., Zhang, X. X., Mao, Y. W., Zhu, Y. Y., Yang, Z. Y., Chan, C. T., and Sheng, P. (**2000**). "Locally resonant sonic materials," Science **289**, 1734–1736.
Ma, G., Yang, M., Xiao, S., Yang, Z., and Sheng, P. (**2014**). "Acoustic metasurface with hybrid resonances," Nat. Mater. **13**, 873–878.
Maa, D. (**1975**). "Theory and design of microperforated panel sound-absorbing constructions," Sci. Sin. **18**, 55–71.
Maa, D. (**1998**). "Potential of microperforated panel absorber," J. Acoust. Soc. Am. **104**, 2861–2866.
Mei, J., Ma, G., Yang, M., Yang, Z., Wen, W., and Sheng, P. (**2012**). "Dark acoustic metamaterials as super absorbers for low-frequency sound," Nat. Commun. **3**, 756.
Ngo, T. D., Kashani, A., Imbalzano, G., Nguyen, K. T. Q., and Hui, D. (**2018**). "Additive manufacturing (3D printing): A review of materials, methods, applications and challenges," Compos. Part B Eng. **143**, 172–196.
Popa, B.-I., Zigoneanu, L., and Cummer, S. A. (**2011**). "Experimental acoustic ground cloak in air," Phys. Rev. Lett. **106**, 253901.
Ryoo, H., and Jeon, W. (**2018**). "Dual-frequency sound-absorbing metasurface based on visco-thermal effects with frequency dependence," J. Appl. Phys. **123**, 115110.
Shao, C., Liu, C., Ma, C., Long, H., Chen, K., Cheng, Y., and Liu, X. (**2021**). "Multiband asymmetric sound absorber enabled by ultrasparse Mie resonators," J. Acoust. Soc. Am. **149**, 2072–2080.
Tijdeman, H. (**1975**). "On the propagation of sound waves in cylindrical tubes," J. Sound Vib. **39**, 1–33.
Toyoda, M., Sakagami, K., Takahashi, D., and Morimoto, M. (**2011**). "Effect of a honeycomb on the sound absorption characteristics of panel-type absorbers," Appl. Acoust. **72**, 943–948.
van der Eerden, F. (**2000**). "Noise reduction with coupled prismatic tubes," Ph.D. thesis, University of Twente, Enschede, Netherlands.
Wang, Y., Zhao, H., Yang, H., Zhong, J., Zhao, D., Lu, Z., and Wen, J. (**2018**). "A tunable sound-absorbing metamaterial based on coiled-up space," J. Appl. Phys. **123**, 185109.
Wu, F., Xiao, Y., Yu, D., Zhao, H., Wang, Y., and Wen, J. (**2019**). "Low-frequency sound absorption of hybrid absorber based on micro-perforated panel and coiled-up channels," Appl. Phys. Lett. **114**, 151901.
Xie, Y., Popa, B.-I., Zigoneanu, L., and Cummer, S. A. (**2013**). "Measurement of a broadband negative index with space-coiling acoustic metamaterials," Phys. Rev. Lett. **110**, 175501.
Xie, Y., Wang, W., Chen, H., Konneker, A., Popa, B.-I., and Cummer, S. A. (**2014**). "Wavefront modulation and subwavelength diffractive acoustics with an acoustic metasurface," Nat. Commun. **5**, 5553.
Yang, M., Chen, S., Fu, C., and Sheng, P. (**2017**). "Optimal sound-absorbing structures," Mater. Horiz. **4**, 673–680.
Zhang, Q., Zhang, K., and Hu, G. (**2016**). "Smart three-dimensional lightweight structure triggered from a thin composite sheet via 3D printing technique," Sci. Rep. **6**, 22431.
Zhu, J., Christensen, J., Jung, J., Martin-Moreno, L., Yin, X., Fok, L., Zhang, X., and Garcia-Vidal, F. J. (**2011**). "A holey-structured metamaterial for acoustic deep-subwavelength imaging," Nat. Phys. **7**, 52–55.
Zwikker, C., and Kosten, C. W. (**1949**). *Sound Absorbing Materials* (Elsevier, New York).